

NONLINEAR OPTICAL PHENOMENA

PACS numbers: 42.55.Wd; 42.60.Da; 42.60.Lh; 42.65.Ky
DOI: 10.1070/QE2012v042n10ABEH014829

Cascaded frequency doublers for broadband laser radiation

N.F. Andreev, K.V. Vlasova, V.S. Davydov, S.M. Kulikov, A.I. Makarov, S.A. Sukharev, G.I. Freidman, S.V. Shubin

Abstract. **A new scheme of a cascaded converter of the first harmonic of broadband cw laser radiation into the second harmonic (SH) with compensation for the group walk-off in cascades is proposed and investigated. The conditions under which high conversion coefficients of broadband (~33 cm^{-1}) single-mode fibre laser radiation with low peak power (~300 W) into the SH are determined for frequency doublers based on the most promising LBO crystal. Conversion of cw radiation with an average power of 300 W and efficiency η = 4.5% into the SH is obtained in a single LBO crystal. Effect of coherent addition of SH radiation excited in different cascades is demonstrated for two- and three-stage schemes. The expected conversion efficiencies, calculated disregarding loss but taking into account real aberrations of elements, are 18% and 38%, respectively. The effect of pumping depletion begins to manifest itself in the third cascade of a three-stage converter; it may reduce the latter value to ~30%.**

Keywords: *second-harmonic generation, LBO crystal, angle-noncritical phase matching, spectral phase-matching width, cascaded frequency-doubling scheme, coherent field addition.*

1. Introduction

The progress in the development of high-efficiency cw ytterbium-doped fibre lasers with a working wavelength λ = 1070 nm, a divergence angle close to the diffraction limit, and power on the order of 1 kW opens wide possibilities for their application in high-tech industry and in a number of scientific applications. A promising way for expanding the range of application of such lasers is to convert their radiation into the second harmonic (SH) with a power efficiency of several tens of percent and average power up to several hundreds of watt.

The purpose of this work was to investigate the possibility of efficient conversion of cw ytterbium-doped fibre laser radiation into the SH with a power up to several hundreds of watts by the example of an ytterbium fibre laser (Research Production Enterprise 'IRE-Polus'). The radiation parameters for this laser are as follows: wavelength λ = 1070 nm, nonpolarised radiation, single-mode beam power 600 W (M^2 = 1.08), and spectral width $\Delta f_{1\omega}$ = 33.6 cm^{-1} at the half-maximum level (below all spectral widths are indicated for this level). A specific feature of the problem solved in this study is that the peak power of an isolated polarised component of laser radiation at a large spectral width is low in comparison with the peak power of pulsed lasers. These first-harmonic (FH) parameters do not make it possible to obtain a high conversion efficiency into the SH when using conventional frequency doubling schemes. At the same time, the average power of 100–1000 W calls for minimising the influence of various thermal effects in nonlinear crystals (NLCs) and accompanying optics (lenses, mirrors, polarisers, etc.), which hinder efficient second harmonic generation (SHG).

Currently, the lasers based on active crystal elements [1, 2] with an average power of ~100 W at a wavelength of 530 nm operate in the repetitively pulsed regime at a high peak power (pulse duration 10–30 ps, repetition rate 78–110 MHz) and with a divergence somewhat exceeding the diffraction limit (M^2 = 1.2–2.7). A repetitively pulsed fibre laser with an output power of 60 W at a wavelength of 540 nm (pulse duration 5 ns, repetition rate 10 MHz, M^2 = 1.33) was described in [3]. According to our data, the highest SH power obtained by conversion of cw Nd:YAG laser radiation was reported in [4]: 16 W at M^2 = 1.2 and 27 W at M^2 = 8.

In Section 2 we consider the SHG processes in focused broadband FH beams in the fixed-pump-field approximation. Based on this consideration, we chose a nonlinear LBO crystal optimal for efficient SHG. We also determined the main parameters of a one-stage converter; in particular, the ultimate SH conversion efficiency of the ytterbium fibre laser (IRE-Polus).

In Section 3 we analyse the possibilities of increasing several times the SHG efficiency using two- and three-stage converters with compensation for the relative group walk-off of harmonic waves, which arises during their propagation in the NLC and accompanying optics because of the difference of harmonic group velocities, mounting crystal plates with an appropriate dispersion relation between the NLCs [5]. When this compensation technique is used in a cascaded scheme, an increase in the number N of NLCs does not reduce the spectral phase-matching width [6], whereas the efficiency can be increased by a factor of N^2 in some cases. To implement this concept in practice, we investigated the two-stage scheme presented in Fig. 1a and the LBO-based three-stage scheme. In contrast to [5], where both the spatial walk-off of the SH beam and the temporal group walk-off of harmonics were compensated, we used LBO crystals heated to the noncritical phase-matching temperature, in which relative spatial walk-

N.F. Andreev, K.V. Vlasova, V.S. Davydov, A.I. Makarov, G.I. Freidman, S.V. Shubin Institute of Applied Physics, Russian Academy of Sciences, ul. Ul'yanova 46, 603950 Nizhnii Novgorod, Russia; e-mail: nandreev@appl.sci-nnov.ru;
S.M. Kulikov, S.A. Sukharev Institute of Laser Physics Research, Russian Federal Nuclear Center 'All-Russian Research Institute of Experimental Physics', prosp. Mira 37, 607188 Sarov, Nizhnii Novgorod region, Russia; e-mail: kulikov@otd13.vniief.ru

Received 8 February 2012; revision received 6 June 2012
Kvantovaya Elektronika **42** (10) 887–898 (2012)
Translated by Yu.P. Sin'kov

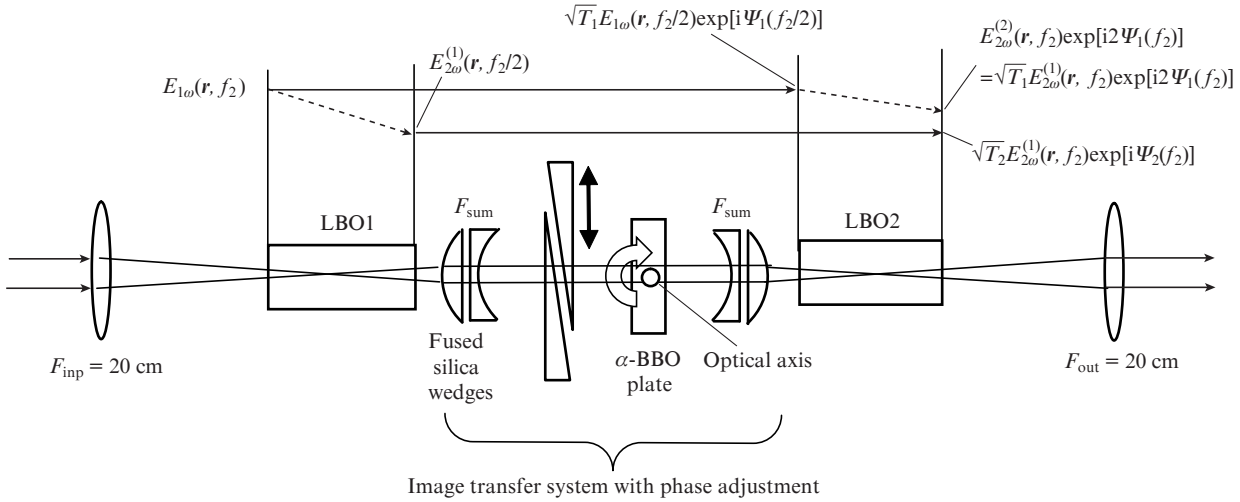

Figure 1. Schematic optical diagram, which clarifies the relationship between the harmonic field structures in different cross sections and the principle of phase compensation, which was applied to determine the α-BBO crystal thickness. The reported relations between the fields suggest exact transfer of the harmonic field structure by the image transfer system from the LBO1 output to the LBO2 output.

off of harmonic waves was absent. This approach allowed us to focus sharply the converted radiation in an NLC to obtain the maximum conversion efficiency for a given crystal length. An optical image transfer system composed of achromatic lenses was used to transfer the FH field structure from the first NLC to the second one. Compensation for the relative group walk-off of waves in the optical system and the phase matching of SH fields at the output of the second NLC were performed using an α-BBO crystal plate, installed between the first and second NLCs. Section 4 contains the results of experimental study of LBO-NLC-based one-, two-, and three-stage frequency doublers of broadband fibre laser radiation. The main results of the study are formulated in the Conclusions.

2. Analysis of frequency doubling for focused broadband radiation

Let us first consider the SHG processes occurring in one crystal. The conversion efficiency into the SH will be calculated in the fixed-field approximation for an FH beam with a Gaussian transverse structure. In this approximation the linear inhomogeneous equation for the SH field is solved in the general case using the Fourier–Laplace transformation in time and transverse coordinates [7]. The transverse structure of the SH-field spectral components for Gaussian (in transverse coordinates) FH beams with a time-dependent complex amplitude $E_{1\omega}(t)$ is determined analytically, as for monochromatic beams [8, 9]. In the case of quasi-stationary dependence of the amplitude $E_{1\omega}(t)$, it is convenient to write the expression for the ratio of the SH power P_2, averaged over time t_{st} (which greatly exceeds the correlation time τ_{cor}), to the average FH power P_1 (the conversion coefficient or conversion efficiency $\eta = P_2/P_1$) in the form

$$\eta = \frac{n_0 K^2}{\lambda_{10} c\varepsilon_0} P_{\text{leff}} \int p_{2\omega}(f_1) S(\Delta k(f_1), \beta_1, \beta_2)\, \mathrm{d}f_1. \qquad (1)$$

Here, $f_1 = \tilde{f}_1 - f_{10}$ is the detuning (in cm^{-1}) of the FH frequency $\tilde{f}_1$ from the carrier frequency f_{10} (the corresponding detuning for the SH frequency f_2 will be larger than f_1 by a factor of 2); $K = 2\pi \times d_{\text{eff}}/\lambda_{10}\sqrt{n_0 n_1 n_2}$; d_{eff} is the coefficient determining the crystal nonlinearity (in m V^{-1}); λ_{10} is the FH wavelength; $\varepsilon_0 = 1/(4\pi 9\times 10^9)$; n_0 is the refractive index for the FH o-wave;

$$P_{\text{leff}} = \frac{(cn_0\varepsilon_0\pi a_0^2/2)\int_{t_{st}} |E_{1\omega}(t)|^4 \mathrm{d}t}{\int_{t_{st}} |E_{1\omega}(t)|^2 \mathrm{d}t},$$

$$p_{2\omega}(f_1) = \frac{|P_{2\omega}(f_1)|^2}{\int |P_{2\omega}(f_1')|^2 \mathrm{d}f_1'}$$

are, respectively, the effective FH power and the normalised spectral intensity of nonlinear polarisation excited at the SH frequency, which depend on the character of time modulation of the FH amplitude; and $P_{2\omega}(f_1)$ is the spectrum of the squared amplitude $E_{1\omega}(t)$, which is proportional to the polarisation induced at the SH frequency. The following relations are valid:

$$\int |P_{2\omega}(f)|^2 \mathrm{d}f = \int_{t_{st}} |E_{1\omega}(t)|^4 \mathrm{d}t$$

and

$$P_{2\omega}(f_1) = \int E_{1\omega}(f_1') E_{1\omega}(f_1 - f_1')\, \mathrm{d}f_1'$$

The function $S(\Delta k, \beta_1, \beta_1)$ coincides with the phase-matching curve for monochromatic waves. For the first- and second-type interactions, it is determined by the relation

$$S(\Delta k, \beta_1, \beta_2) = \sqrt{\frac{2}{\pi}}\frac{z_{\text{d}}}{L_{\text{cr}}} \times \int_{-\infty}^{\infty} \exp\left(-\frac{x^2}{2}\right) \int_{-\frac{L_{\text{cr}}}{2z_{\text{d}}}}^{\frac{L_{\text{cr}}}{2z_{\text{d}}}} \exp\left\{\left[\mathrm{i}(\Delta k z_{\text{d}} + \frac{\beta_2}{\theta}x - \frac{1}{2}\frac{\beta_1}{\theta}x)\tilde{z} - \frac{(\beta_1\tilde{z}/\theta)^2}{4(1-\mathrm{i}\tilde{z})}\right](1-\mathrm{i}\tilde{z})^{-1}\right\} \mathrm{d}\tilde{z}\, |^2 \mathrm{d}x. \qquad (2)$$

Here, it is assumed that the waist is located at the crystal centre, and the following designations are introduced: β_1 and β_2 are the walk-off angles of the FH and SH e-wave beams, respectively; $\theta = \lambda_{10}/2\pi n_0 a_0$ is the diffraction divergence angle of the Gaussian FH beam in the waist of o-wave with a radius a_0 at the 1/e-intensity level; $z_d = (2\pi n_0/\lambda_{10})a_0^2$ is the half-length of the FH o-wave beam waist; L_{cr} is NLC length; $\Delta k = k_2^e - k_1^o - k_1^e$ is the wave detuning for the second-type mismatch; and $\Delta k = k_2^e - 2k_1^o$ for the first-type mismatch. Note that the wave detuning is related, first, to the deviation ΔT of the crystal temperature from optimal (Δk_T); second, to the frequency detuning Δk_f from the peak of the phase-matching curve; and, finally, to the angular detuning Θ of the crystal from the phase-matching angle (Δk_Θ), which are determined for a given propagation direction. Thus, $\Delta k = \Delta k_T + \Delta k_f + \Delta k_\Theta$, where $\Delta k_T \propto \Delta T$, $\Delta k_\Theta \propto \Theta$ (for the angle-noncritical phase matching $\Delta k_\Theta \propto \Theta^2$); $\Delta k_f = 2\pi S_{21} f_2$; $S_{21} = (c/c_{2\omega}^e - c/c_{1\omega}^o)$ and $S_{21} = [c/c_{2\omega}^e - 0.5(c/c_{2\omega}^e + c/c_{1\omega}^o)]$ are the dimensionless group mismatches for the first- and the second-type interactions, respectively; c is the speed of light in vacuum; and c, $c_{1\omega}^e$, $c_{1\omega}^o$, $c_{2\omega}^e$ are the group velocities of harmonic waves in the crystal. In the absence of wave walk-off at $\beta_1, \beta_2 = 0$ (the case of angle-noncritical phase matching), expression (2) coincides with the known expression reported in [9].

As was indicated above, the effective FH power P_{1eff} and the relation between the FH spectrum and the spectrum of nonlinearly polarised $p_{2\omega}(f_2)$ that excites the SH depend on the specific character of FH time modulation. We will only note the general regularities, which are useful for analysing the experimental results and calculating the doubler parameters. Obviously, P_{1eff} is equal to the average FH power P_1 if its modulation is of purely phase type and the ratio of these values increases with an increase in the amplitude modulation depth, which is known to rise (for example, for the Gaussian statistics of the FH field) the conversion efficiency by a factor of 2 [6]. The ratio of the FH spectral width Δf_1 and the spectral width Δf_{2p} of nonlinear polarisation $\Delta f_{2p} \approx 2\Delta f_1$) depends on the character of FH modulation in a more complicated way. In the case of purely phase modulation for a spectrum close to Gaussian, $\Delta f_2 \approx \sqrt{2}\,\Delta f_{1\omega}$, while for purely amplitude modulation $\Delta f_2 \approx \sqrt{2}\,\Delta f_{1\omega}$. If the modulation is of mixed type, the inequality $\Delta f_{2p} > \sqrt{2}\,\Delta f_{1\omega}$ can be implemented; this situation was observed in our experiments (see below). A more detailed discussion of the reasons for the different ratios of the widths under consideration is beyond the scope of this study.

Expression (1) makes it possible to optimise the doubler parameters and estimate the attainable SH power. These possibilities will be demonstrated by the example of a biaxial LBO NLC, the z axis of which lies in the input plane ($\Theta = 90°$) and the FH and SH wave vectors are parallel to the x axis ($\varphi = 0$). When this crystal has a temperature close to $T_{crit} \approx 141.8\,°C$ (it was calculated using the SNLO code [10]), it implements angle-noncritical phase matching of the first type, o + o → e ($d_{eff}^{LBO} = 0.849$ pm V^{-1} at a temperature of 140 °C) [10]. As will be shown below, this crystal is most promising for frequency doublers of broadband radiation with an average power of 10^2–10^3 W. The crystal length L_{cr} was 15 mm both in the calculations and in the experiment. The characteristics of FH radiation in the calculations were chosen close to the experimentally implemented ones: $P_{1\omega} = 300$ W and $\Delta f_1 = 33.6$ cm^{-1}. Since there was no data on the contribution of amplitude modulation to the FH spectral width, the FH radiation with $\lambda_{10} = 1070$ nm was assumed to be phase-modulated and have a Gaussian spectrum. Below we will compare the results of these calculations with the experimental data. It was also assumed that the crystal temperature is close to the noncritical phase-matching temperature $T_{crit} \approx 141.8\,°C$ and $\beta_1 = \beta_2 = 0$. According to [10], the group refractive indices $n_{g1} = c/c_{1\omega}^o$ и $n_{g2} = c/c_{2\omega}^e$ are, respectively, 1.626 and 1.638 at this temperature.

Figure 2 shows the dependences of the conversion efficiency on the radius a_0 of the beam waist, located at the NLC centre, for monochromatic and broadband ($\Delta f_1 = 33.6$ cm^{-1}) FH radiations. According to these dependences, the conversion coefficient for monochromatic radiation reaches a maximum at $a_0 = a_{0m} = 16.7$ μm (the corresponding waist length $2z_d = 5.5$ mm) and is equal to 6.6%. For broadband radiation the maximum is obtained in a more focused beam ($a_0 = a_{0b} = 15$ μm) and amounts to 4.5%. The η value decreases due to the increase in the phase-matching width with a decrease in z_d (Fig. 3); in particular, at $a_0 = a_{0b}$ the phase-matching width $\Delta f_{s1} = 30.9$ cm^{-1}, whereas at $a_0 = a_{0m}$ it is 29.8 cm^{-1}. It also follows from Fig. 3 that focusing shifts the phase-matching curve. Using the data of Ref. [10], one can easily calculate the so-called temperature-dispersion coefficient, which relates the change in the noncritical phase-matching temperature to the FH frequency shift: $\alpha_{Tf} = 0.139\,°C$ cm. Based on this value and the calculated shifts of the centre of the phase-matching curve with a change in a_0, we find that the optimal temperature for focused beams is lower than the value calculated using the data [10] by 1.8 °C and should be equal to 140 °C.

Figure 4 shows the results of calculating the maximum conversion efficiency of broadband radiation for an LBO crystal, which is obtained at optimal focusing and optimal temperature and depends on the crystal length L_{cr}. According to these calculations, at a crystal length of 30 mm the maximum efficiency for radiation with a spectral width of 33.6 cm^{-1} is 5.5% and increases very slowly with a further increase in L_{cr}. Having divided a 30-mm-long LBO crystal into two crystals of equal length and used them in the proposed scheme, one can obtain (disregarding the nonlinear saturation effects) a SH conversion coefficient exceeding the one-crystal value

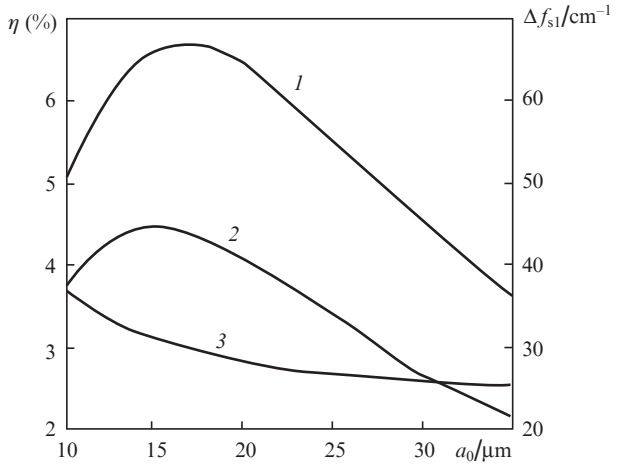

Figure 2. Calculated dependences of the conversion efficiency in a 15-mm-long LBO crystal under conditions of noncritical phase matching on the beam radius in the waist for (*1*) monochromatic FH radiation with a power of 300 W and (*2*) phase-modulated FH radiation with a spectral width of 33 cm^{-1} and (*3*) the dependence of the spectral phase-matching width Δf_{s1} on a_0.

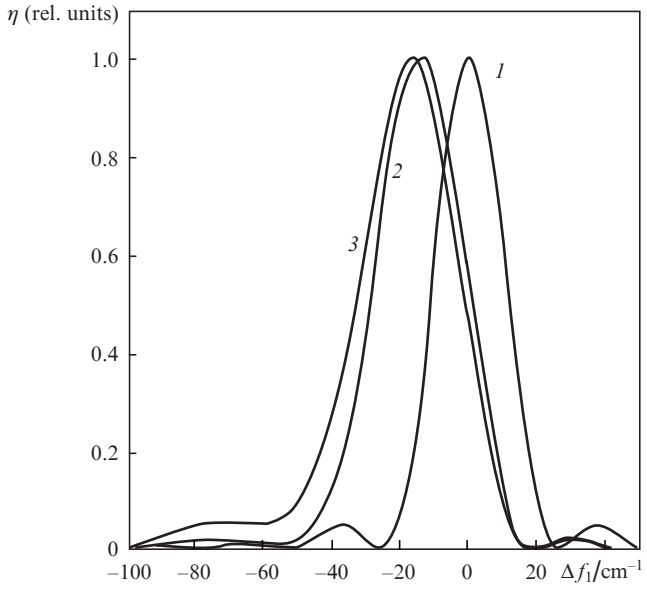

Calculated normalised dependences of the conversion efficiency in a 15-mm-long LBO crystal (*1*) under conditions of noncritical phase matching on the frequency detuning from the central frequency of the FH phase matching (phase-matching curves) in the plane-wave approximation ($\Delta f_{s1} \approx 24.6$ cm^{-1}), (*2*) at optimal focusing for a monochromatic wave with $a_0 = 16.7$ μm ($\Delta f_{s1} \approx 29.8$ cm^{-1}), and (*3*) at focusing of broadband radiation with a waist $a_{0b} = 14$ μm ($\Delta f_{s1} \approx 30.9$ cm^{-1}).

by a factor of 4: $\eta = 4.5\% \times 4 = 18\%$. This gain indicates good prospects of our method for doubling the frequency of broadband low-power radiation using cascaded schemes.

Here, we should consider the ratio of the FH power density in the obtained optimal beam geometry to the value at which LBO crystal undergoes breakdown. In accordance with the data reported in [10] and recalculated using the root dependence of this value (from a duration of 10 ns (25 J cm^{-2}) to 100 μs (experimental duration)), the 'breakdown' power density is 25 MW cm^{-2}. As far as we know, there are no data in the literature on the corresponding value for cw radiation. On the other hand, the power densities in the beam waist and on the crystal surface in the geometry under consideration at an FH power of 300 W are, respectively, 42.4 and 3.1 MW cm^{-2}; i.e., the power density on the surface is an order of magnitude smaller than in the bulk. At the same time, the latter value exceeds that calculated from the root dependence by a factor of almost 2. The inconsistency of these data made us choose experimentally the corresponding parameters (see Section 4).

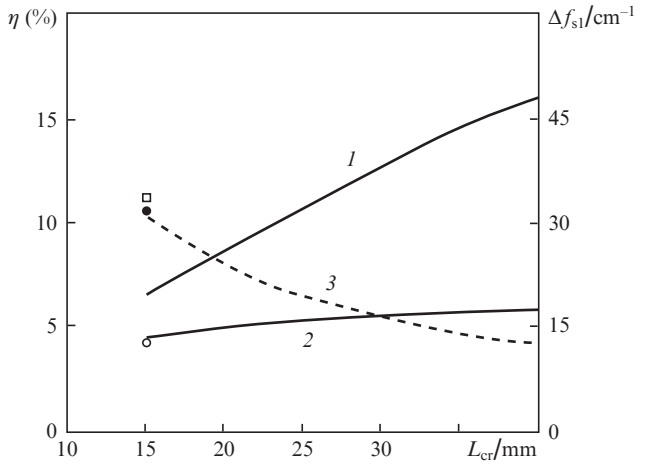

Figure 3. Calculated dependences of the conversion efficiency in an LBO crystal on its length, at an FH power of 300 W and under conditions of optimal beam radius in the waist in the maximum of phase-matching curve for each length: (*1*) monochromatic radiation, (*2*) broadband radiation with a spectral width of 33 cm^{-1}, and (*3*) the corresponding width of spectral phase matching. The symbols show the experimental values of the efficiency (○), phase-matching width (●), and spectral width of converted radiation (□).

A similar analysis was performed for doublers based on β-BBO and KTP crystals, the nonlinearity in which greatly exceeded that in the LBO crystal ($d_{\text{eff}}^{\text{BBO}} = 2.01$ pm V^{-1} [10], $d_{\text{eff}}^{\text{KTP}} = 3.18$ pm V^{-1} [11, 12]). However, the β-BBO crystal [below we consider the first-type phase matching (o + o → e), characterised by the highest nonlinearity, for this crystal] exhibits a group-velocity mismatch exceeding that in LBO by a factor of 2 ($S_{21}^{\text{BBO}} \approx 0.025$) and a rather large birefringence angle ($\beta_2^{\text{BBO}} = 55.6$ mrad). Therefore, according to the calculation, the conversion efficiency for broadband radiation at optimal focusing in the maximum of the phase-matching curve and at the β-BBO-crystal length $L_{\text{cr}} = 15$ mm is only 1.6%.

The influence of birefringence can significantly be reduced using an assembly of several crystals, cut under the phase-matching angle and closely coupled, with relative arrangement of axes leading to compensation for the spatial walk-off of harmonics but retaining the nonlinearity sign [5, 6]. We performed a calculation to estimate the conversion efficiency for this optical design with a total length of 5.4 mm and different numbers of domains N. For this design, independent of N, the resulting spectral phase-matching width was ~34 cm^{-1}. The beam radius was assumed to be 35.9 μm in the calculation, a value corresponding to the power density on the surfaces of assembly-forming crystals that amounts to 0.6 of the 'breakdown' density power, recalculated from the root dependence on the duration from 10 ns (13 J cm^{-2} for the BBO crystal [10]) to 100 μs (1.3×10^7 W cm^{-2}). As a result, the efficiency for different N values (from 11 to 53) was ~2.4%. Note that the low conversion efficiency for this design is determined to a great extent by the radiation resistance of the β-BBO crystal.

For the KTP crystal the effect of beam spatial walk-off is insignificant (phase matching of the e + o → e type; the birefringence angles, according to [10], are 2.95 and 3.89 mrad for FH and SH, respectively); however, the group mismatch is larger than that for LBO by a factor of about 6 ($S_{21}^{\text{KTP}} \approx 0.0745$). The crystal thickness at which the phase-matching width is ~34 cm^{-1} amounts to ~1.6 mm, and the conversion efficiency at a power density equal to half breakdown value is 0.43%. Here, the beam radius a was assumed to be 35.7 μm, and the power density, recalculated from the root dependence from 10 ns (15 J cm^{-2} for the KTP crystal [10]) to 100 μs, was 1.5×10^7 W cm^{-2}. At first glance, the efficiency can be increased by increasing the crystal length. All the more so, the beam radius a_0 in the waist can be reduced, with preservation of its value on the crystal surface, because the breakdown power density in the crystal bulk greatly exceeds that on the surface. According to the calculation in the fixed-field approximation at $L_{\text{cr}} = 9$ mm and $a_0 = 14$ μm, the efficiency is 8.6%, i.e., higher by a factor of 2 than in the 15-mm-long LBO crystal at that same radius a_0. (Note that, as our studies showed, in this beam geometry, at a pulse width of 100 μs, the FH power

density on the input surface of KTP crystal is close to the aforementioned 'breakdown' value.) However, in this case the spectral phase-matching width is much smaller than the spectral width of the converted radiation and is equal to 7.6 cm^{-1}. The conversion efficiency for monochromatic radiation reaches 38.9% at this focusing. Obviously, the fixed-pump-field approximation is invalid under these conditions. A correct (and fairly complicated) calculation under conversion-saturation conditions requires information about the temporal structures of the amplitude and phase modulations of fibre laser radiation, which are unknown to us. Below we present the experimental dependences of the SH conversion efficiency in a KTP crystal on the power of broadband fibre laser radiation, which demonstrate conversion saturation in a 9-mm-long KTP at a level of 3.8%.

In addition, KTP is characterised by rather strong absorption ($\alpha_{KTP} \sim 10^{-2}$ cm^{-1} at the SH frequency and $\alpha_{KTP} \sim 10^{-4}$ cm^{-1} at the FH frequency). Therefore, implementation of high conversion efficiencies will cause a temperature drop $\Delta T \approx 6-12$ °C in the region of the waist of a focused cw FH beam with a power $P_1 = 300-600$ W in the transverse direction; this drop is comparable with the temperature phase-matching half-width $\Delta T \approx 11.4$ °C [10]. As a result, the conversion efficiency significantly decreases and the crystal may be destroyed by thermally induced stresses.

Thus, based on the results of the calculations and experimental studies and in view of the existence (according to the data of [13]) of LBO crystals with $\alpha_{LBO} \leqslant 10^{-5}$ cm^{-1} (heating by cw laser radiation with a power of ~1000 W is negligible for these crystals), which was indirectly confirmed in our studies, LBO crystals are most promising for broadband doublers with power P_1 in the range from 100 to 1000 W.

3. Two- and three-stage frequency doublers with image transfer systems

As was indicated in the Introduction, a SH conversion efficiency of more than 5% for broadband (up to 34 cm^{-1}) high-power cw fibre laser radiation can be reached using only a cascaded scheme, composed of two or more LBO NLCs.

Figure 1 shows a schematic diagram of a two-stage converter. A fused silica lens with a focal length $F_{inp} = 20$ cm, mounted at the optimal distance from the collimating objective, focuses FH radiation into an LBO crystal with a length of 15 mm and an aperture of 3×3 mm to form a waist of radius $a_0 = 13.9$ μm in its middle. In our experiment the crystal was heated to 140.2 °C, a temperature corresponding to the maximum conversion efficiency. This value is close to the calculated one (140 °C), at which the maximum efficiency is implemented in an optimally focused beam near noncritical phase matching.

An image transfer system was placed behind the first LBO crystal; its first lens was installed so as to make the FH radiation at its output collimated. An α-BBO crystal plate with an appropriate orientation of axes and two oppositely directed fused silica wedges were located between the image transfer system lenses. This design served, first, to match the phases of the SH fields at the output of the second NLC and, second, to compensate for the group walk-off of the temporal structures of harmonics in nonlinear crystals and in the image transfer system lenses. The beam collimation in the image transfer system excluded the dependence of the phase correction introduced by the optical elements on the transverse coordinate. The image transfer system lenses had identical focal lengths F_{sum} for the FH and SH and were composed of two lenses: negative (made of fused silica) and positive (made of crystalline quartz). The optical axis of the latter was in the lens plane and coincided with the SH-polarisation direction. The radii of curvature of the lenses were calculated from the condition of equal focal lengths F_{sum} at the FH and SH wavelengths.

In the fixed-field approximation the FH in the first and second NLCs propagates as in a linear medium. In turn, the spatial structure of the SH field in the second NLC (LBO2) can be presented as a sum of two fields: the SH field, which is generated in the first NLC (LBO1) (it does not undergo nonlinear distortion in the second NLC and propagates as in a linear isotropic medium), and the SH field, which is generated in LBO2 [14].

The relative arrangement of the image transfer system and nonlinear crystals is chosen so as to make the spatial structure of the FH field $E_{1\omega}(\boldsymbol{r}, f_2/2)\exp[i\Psi_1(f_2/2)]$ at the LBO2 input identical [accurate to the phase factor $\Psi_1(f_2/2)$] to the corresponding field at the LBO1 input: $E_{1\omega}(\boldsymbol{r}, f_2/2)$. Here, f_2 is the SH frequency detuning from the carrier frequency, and the frequency dependence of the field is related to the nonmonochromaticity of laser radiation. The spatial structure $E^{(2)}_{2\omega}(\boldsymbol{r},f_2)\exp(i2\Psi_1(f_2))$ of the SH field generated in LBO2 at its output is identical (accurate to the phase factor) to the $E^{(1)}_{2\omega}(\boldsymbol{r},f_2)$ structure of the SH field at the LBO1 output. This is due to the identity of the FH field structures at the inputs of the LBO1 and LBO2 crystals and to the absence of transverse walk-off of the extraordinary SH wave under conditions of noncritical phase matching. In addition, the $E^{(2)}_{2\omega}(\boldsymbol{r},f_2) \times \exp(i2\Psi_1(f_2))$ field is similar to the $E^{(1)}_{2\omega}(\boldsymbol{r},f_2)\exp(i2\Psi_2(f_2))$ field, generated in LBO1 and transmitted through the image transfer system and LBO2. This result is provided by the achromatism of the image transfer system lenses and the corresponding tuning of the image transfer system, as well as by the equality of the refractive indices in the NLC under phase-matching conditions for the FH and SH (this equality ensures identical conversion of FH and SH fields by the image transfer system within the NLC). Therefore, the SH field in some arbitrary cross section at the output of two-stage scheme is the sum of fields with identical spatial structures but different powers (due to the linear loss in the image transfer system) and phase factors, related to the linear phase shift of harmonics during their propagation in the image transfer system elements and crystals. Using the designations from Fig. 1 (T_2 is the transmittance of the scheme elements for the SH radiation generated in the first NLC and T_1 is the transmittance of the FH power through the image transfer system), one can write the relation

$$E^{(2)}_{2\omega}(\boldsymbol{r},f_1) = T_1 E^{(1)}_{2\omega}(\boldsymbol{r},f). \tag{3}$$

The axial phases $\Psi_{1,2}(f_2)$ of the SH fields at the output of the second crystal are determined by the phase shift during wave propagation in the linear media of the image transfer system elements and in the LBO crystals. Note that, along with the aforementioned phase shift during harmonic excitation, there are additional phase shifts of the SH fields in the NLC:

$$\varphi^{nl}_{1,2}(f_2) = \arg\left[\int_{-\frac{L_{cr}}{2z_d}+\Delta x_{1,2}}^{\frac{L_{cr}}{2z_d}+\Delta x_{1,2}} \frac{\exp(i\Delta k(f_2) z_d \tilde{z})}{1-i\tilde{z}} d\tilde{z}\right],$$

where $\Delta x_{1,2}$ are the displacements of the FH beam waist from the centre in the first and second NLCs, respectively (here, as previously, the crystal lengths are assumed to be identical).

The formula for $\varphi^{nl}_{1,2}(f_2)$ stems from the expression for the SH field excited by a focused Gaussian beam under noncritical phase matching conditions [9]. At $\Delta x_{1,2} = 0$, $\varphi^{nl}_{1,2}(f_2) = 0$ in Gaussian beams. Note also that, when the image transfer system is correctly tuned, the relation $\varphi^{nl}_1(f_2) - \varphi^{nl}_2(f_2) = 0$ is valid for an arbitrary Δx value; i.e., these phases should not affect the coherent addition of SH fields at the output of the scheme. The aforementioned property of SH generation must be taken into account when aligning both the waist position in the NLC and the relative arrangement of the NLC and image transfer system, because the frequency dependence $\varphi^{nl}_1(f_2) - \varphi^{nl}_2(f_2)$ within the phase-matching width cannot be presented as a linear dependence on f_2 (Fig. 5). Further analysis of the coherent addition of SH fields is based on this circumstance.

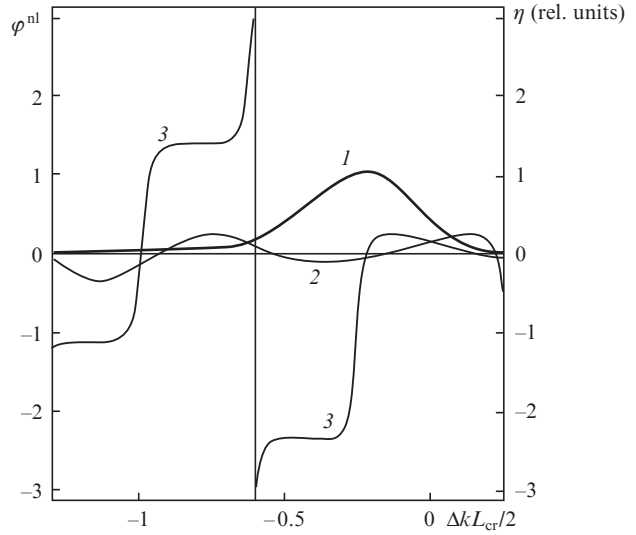

Figure 4. Dependences of the (*1*) normalised efficiency at frequency doubling for a beam with a radius of 13.9 μm in the waist and (*2*, *3*) φ^{nl} at a waist shifted from the center by 1.5 mm to the (*2*) output and (*3*) input surfaces in a 15-mm-long LBO crystal on the wave mismatch.

For a three-stage converter the emission of harmonics from the output of the second cascade to the third cascade is presented similarly.

Using the designations introduced, we will write the expression for the SH spectral intensity in some cross section at the output of the second NLC as the sum of the SH fields excited in the first and second crystals:

$$I_2(\boldsymbol{r}, f_2) = \frac{c\varepsilon_0}{2}\left| T_1 E^{(1)}_{2\omega}(\boldsymbol{r}, f_2)\exp(\mathrm{i}2\Psi_1(f_2)) + \sqrt{T_2}\,E^{(1)}_{2\omega}(\boldsymbol{r}, f_2)\exp(\mathrm{i}\Psi_2(f_2))\right|^2. \quad (4)$$

Obviously, $I_2(\boldsymbol{r}, f_2)$ depends on the field phase difference $\Delta\Psi(f_2) = -2\Psi_1(f_2) + \Psi_2(f_2)$. In the first-order expansion in powers of f, this phase difference can be written as $\Delta\Psi(f_2) = 2\pi\Delta_\Sigma f_2 + \Delta\Psi(0)$. Here, $\Delta_\Sigma = \sum_i S_{21;i}L_i$, $S_{21,i} = c/(c^{e}_{2\omega})_i - c/(c^{o}_{1\omega})_i$ is the normalised group mismatch in the first NLC ($i = 0$) and in different image transfer system elements ($i \neq 0$) and L_i are the lengths of the corresponding elements along the beam axis. For the α-BBO crystal, when the SH is an e-wave and the FH is an o-wave, $S_{21,\,BBO} < 0$, whereas $S_{21,\,i} > 0$ ($i \neq 0$). The phase mismatch of carrier frequencies is $\Delta\Psi(0) = \sum_i \Delta k_i L_i$, where $\Delta k_i = (2\pi/\lambda_{20})[n_i(\lambda_{20}) - n_i(\lambda_{10})]$ is their wave mismatch in the corresponding elements and $n_i(\lambda)$ are the refractive indices of the elements at the corresponding wavelengths.

It follows from expression (4) that, if the thickness of the α-BBO crystal plate is chosen so as to satisfy simultaneously the relations $\Delta_\Sigma = 0$ and $\Delta\Psi(0) = 2\pi m$ and, thus, $\Delta\Psi(f_2) = 2\pi m$ (m is an integer), the harmonic phase mismatch at the output of the second NLC will be compensated for at all frequencies within the radiation spectral band. As a result, we have coherent addition of the complex amplitudes of the SH fields (excited in the two NLCs by the broadband FH field) at the output of the second NLC. Ideally, at $T_1 = T_2 = 1$, we obtain (in the low-power approximation) a fourfold increase in the SH generation efficiency in the two-stage scheme under consideration.

In the case of compensated group mismatch ($\Delta_\Sigma = 0$), the expression for the total SH power $P_{1,2s}(\Psi(0))$ at the output of the second NLC as a function of phase mismatch, which is also valid for non-Gaussian beams in the presence of loss, misadjustment, and image transfer system aberrations, can be written as

$$P_{1,2}(\Psi(0)) = P_2^{(1)} + P_2^{(2)} + 2H_{1,2}\sqrt{P_2^{(1)}P_2^{(2)}}\cos(\Psi(0)). \quad (5)$$

Expression (5) is derived from (4) by integrating over all frequencies and spatial coordinates $\boldsymbol{r}$. Here, $P_2^{(1)}$ and $P_2^{(2)}$ are the real SH powers at the output of the scheme, excited in the first and second crystals, respectively. These values can be measured in a real scheme using successive detuning of nonlinear crystals from phase matching by changing their temperature. The field overlap factor in the last term of (5),

$$H_{1,2} = \frac{c\varepsilon_0}{2}\mathrm{Re}\left\{\int\int E^{(1)}_{2\omega}(\boldsymbol{r},f_2)[E^{(2)}_{2\omega}(\boldsymbol{r},f_2)]^*\,\mathrm{d}\boldsymbol{r}\mathrm{d}f_2\right\} \times\left[\int\int|E^{(1)}_{2\omega}|^2\mathrm{d}\boldsymbol{r}\mathrm{d}f_2\int\int|E^{(2)}_{2\omega}|^2\mathrm{d}\boldsymbol{r}\mathrm{d}f_2\right]^{-1/2} \leqslant 1,$$

characterises the degree of spatial and frequency overlap of the SH beams excited in the first and second NLCs in the presence of aberrations in the optical scheme. This parameter can be determined based on the measured value of the minimum SH power, obtained by changing the phase mismatch $\Psi(0)$ from 0 to π. This transformation in the scheme under consideration was performed by rotating the compensating α-BBO crystal plate around the optical axis. In this case, the phase mismatch ($\Delta k_{BBO}L_{BBO}$) changes, while the group mismatch Δ_Σ barely varies. Note that determination of $H_{1,2}$ from the results of maximum SH quenching at the output [minimum in dependence (5) at $\Psi(0) = \pi$] guarantees a minimum contribution of the FH depletion effect to the measurement of $H_{1,2}$ at summary-harmonic generation in the second crystal. At significant conversion efficiencies, which can be observed in a cascaded scheme in the interference maximum (at $\Psi(0) = 0$), formula (5) yields smaller $H_{1,2}$ values, which is related to the FH depletion in the output crystal and the corresponding distortion of the spatial distributions of the SH interfering fields.

For a three-stage converter with compensation for the group and phase mismatches in the third cascade, the SH power at the output is also determined by expression (5). Here, the $P_2^{(1)}$ value is replaced by $P_{1,2}$ (the power generated by the two-stage scheme at the output of the third cascade with the third NLC switched off), $P_2^{(2)}$ is replaced by $P_2^{(3)}$ (the power at the output of the third NLC when the first two are mismatched), and $H_{1,2}$ is replaced by $H_{1,2,3}$. It should be noted that the field overlap factor in expression (5) will differ from unity due to the violation of equality (3) for the following reasons.

(1) Achromatism of the image transfer system lenses for only two wavelengths: 1070 and 535 nm. When the frequency deviates from these values within the phase-matching spectral band, a difference in the curvatures of the SH beam wavefronts arises at the image transfer system output. This effect is absent for reflecting focusing optics.

(2) Difference in the refractive indices of the optical elements located between the image transfer system lenses at the FH and SH frequencies. This effect will be less pronounced in the scheme without quartz wedges, with a thinner α-BBO crystal, and in the case of longer focal-length image transfer system lenses.

(3) Optical aberrations of the image transfer system.

All the aforementioned distortions in our scheme, as follows from the measurement results (presented below), are in the allowable range.

4. Experimental study

Figure 1 shows a schematic diagram of a two-stage frequency doubler (see above). Nonlinear LBO crystals are heated to the noncritical phase-matching temperature; thus, there is no relative spatial walk-off of harmonic waves in them. Hence, one can sharply focus the converted radiation in the NLC to obtain the maximum (for a given crystal) conversion-efficiency length. An optical image transfer system, composed of achromatic lenses, is used to transfer the FH field structure from the first NLC to the second NLC. Compensation of the relative temporal walk-off of waves in the optical system and matching the SH field phases at the LBO2 output is performed by a α-BBO crystal plate mounted in the image transfer system.

4.1. Single-stage frequency doubler

The FH radiation source was an ytterbium-doped fibre laser (LS-1-C/06-OM, Research Production Enterprise 'IRE-Polus'), generating a depolarised single-mode beam with power up to 600 W at the wavelength $\lambda = 1070$ nm. In addition to the cw regime, the laser could operate in the repetitively pulsed regime due to the modulation of the pump-diode currents by close-to-rectangular pulses of required repetition rate and duration. The studies in the repetitively pulsed regime were performed with laser pulses having a width of 100–300 μs, repetition rate of 10 Hz, and peak power up to 300 W, in linearly polarised light, selected by a polariser. The average power did not exceed 1 W; this limitation excluded the influence of thermal effects in the optical elements in this stage of studies. We performed experiments on LBO and KTP crystals with lengths of 15 and 9 mm, respectively. In the cw regime only the conversion efficiency in a single LBO NLC was measured.

Laser radiation was focused by a fused silica lens ($F_{\text{inp}} = 20$ cm) to the centre of LBO NLC with a length of 15 mm and cross section of 3×3 mm or to the centre of 9-mm-long KTP crystal. The LBO crystal was placed in a thermostat, the temperature of which was varied with a step of 0.1 °C in the range from 140 to 150 °C and maintained constant with an error of ±0.05 °C. The lens focal length and temperature were chosen so as to make maximum the conversion coefficient η to the SH in the LBO crystal at the maximum average power of the polarised component: $P_1 = 300$ W. In the cw regime we had $\eta_{\text{cw max}} = 4.2\% - 4.5\%$; the optimal radius of the FH beam in the waist was $a_{0\,\text{opt}} = 13.9$ μm. These values are close to the above-calculated optimal values for the LBO crystal. They did not change after the polariser was removed and the total power of the radiation transmitted through the waist reached 600 W and the power density in the waist centre amounted to 100 MW cm^{-2}. The FH and SH emission spectra were close to Gaussian, with the widths $\Delta f_1 = 33.6$ cm^{-1} and $\Delta f_2 \approx 46$ cm^{-1} in the LBO crystal.

In the repetitively pulsed regime the maximum conversion efficiency in LBO was measured to be 3.4%; it increased to 4.5% with an increase in the pulse duration to 300 μs and a transition to the cw regime. The difference in the efficiencies is likely to be due to the transient processes during lasing in the repetitively pulsed regime, which occur in the beginning of each pulse; they manifested themselves in the oscillograms of both harmonics [15].

Figure 6 shows the dependences of the FH and SH spectral widths in the LBO crystal on the lasing power, which were measured in the repetitively pulsed regime using 100-μs pulses. The same regime was used to obtain the dependences of the conversion coefficient on the peak power in LBO (Fig. 7) and KTP (Fig. 8) for two ways of changing power. Curves (*1*) in Figs 7 and 8 are the dependences $\eta(P_1)$ obtained at variation in the lasing power and lasing spectral width by changing the pump diode current. Curves (*2*) and (*3*) in

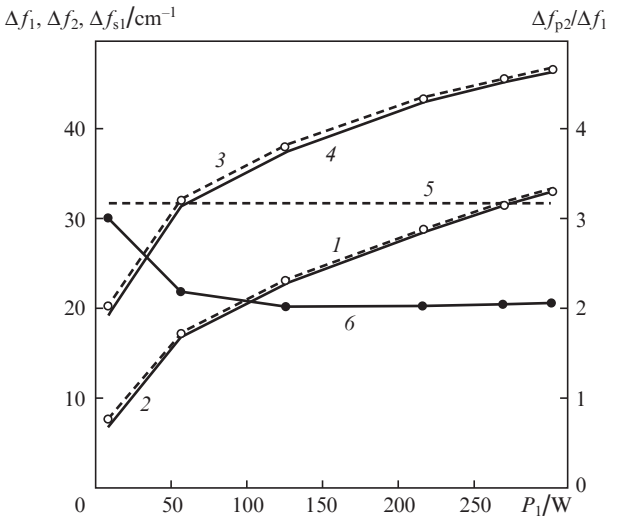

Figure 5. Dependences of the measured (*1*) FH and (*3*) SH spectral widths in an LBO crystal on the lasing power and (*2*, *4*) the same dependences correlated to the instrumental function, (*5*) the phase-matching width at the FH frequency and a 14-μm beam radius in the waist, and (*6*) the ratio of the polarisation power spectral width at the SH frequency to the FH spectral width.

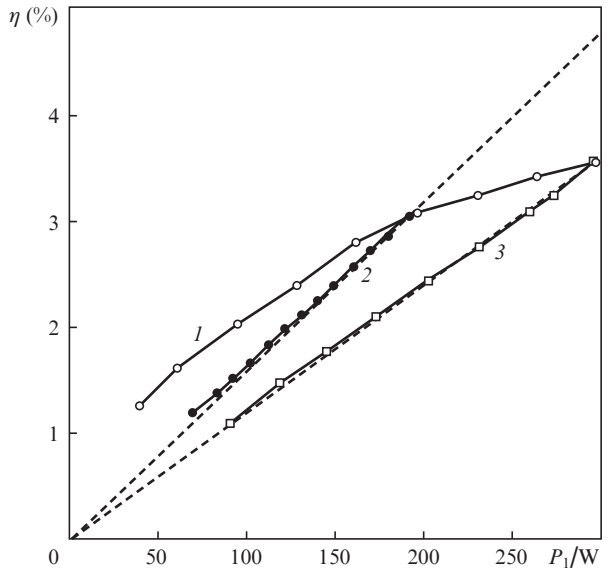

Figure 6. Experimental dependences of the SH conversion efficiency in an LBO crystal (*1*) on the lasing power in the repetitively pulsed regime and (*2*, *3*) on the FH power in the LBO crystal at a specified lasing power and FH spectral widths of (*2*) 27 and (*3*) 33.6 cm^{-1}.

Figs 7 and curve (*2*) in Fig. 8 were obtained under the following conditions: the pump diode current remained constant, as well as the lasing power and spectral width at the output, whereas the FH power applied to the NLC was controlled using a polarisation attenuator. The linearity of these dependences for the LBO crystal, in correspondence with the SHG theory in the fixed-field approximation, indicates weak influence of the saturation effect on the conversion regime in this crystal at the efficiencies observed. In contrast to this, one can clearly see that curve (*2*) in Fig. 8 is nonlinear, which is indicative of strong influence of the saturation effect in the KTP crystal at $\eta(P_1) \approx 3.8\%$. Hence, this crystal cannot be used in the cascaded schemes proposed here.

In the experiments the power density in the beam waist was $I_{waist} = 50$ MW cm^{-2}, while the power density on the input and output crystal surfaces was $I_{inp} = 7$ MW cm^{-2}. However, even at doubled intensities and long ($\sim 10^6$ pulses) laser operation in the repetitively pulsed regime, as well as in the cw regime, the LBO crystal was not destroyed, whereas in the case of KTP crystal operation in the repetitively pulsed regime at a power density of 7 MW cm^{-2} for a rather short time led to characteristic fracture of the crystal surface.

The dependences presented in Fig. 6 make it possible to determine the type of modulation of laser radiation when its power is changed. To this end, one must find the dependence of the width of nonlinear polarisation spectrum $p_{2\omega}$ on f_2. The SH spectrum is proportional to the product of the spectrum $p_{2\omega}(f_2)$ by the phase-matching curve, and all these dependences are close to Gaussian in the central part. Therefore, the width of the spectrum $p_{2\omega}(f_2)$ can be calculated from the relation $\Delta f_{p2} = [(\Delta f_2)^{-2} - (2\Delta f_{s1})^{-2}]^{-1/2}$. The thus obtained dependence of the ratio $\Delta f_{p2}/\Delta f_1$ on power at $\Delta f_{s1} = 30.9$ cm^{-1} is shown in Fig. 6 [curve (*6*)]. It suggests that, at a high laser power, the modulation of laser radiation is close to phase modulation, because $\Delta f_{p2}/\Delta f_{1\omega} \approx 2$. With a decrease in power, this ratio increases to 3, which indicates occurrence of additional amplitude modulation. This is confirmed by the analysis of the dependences of the conversion efficiency on the FH power at different ways of its variation (Figs. 7, 9). For example, the dependence (*2*) in Fig. 9, plotted in correspondence with the linear theory, shows that at a spectral width of about 6 cm^{-1} and a power of 300 W, one would obtain a conversion efficiency of ~9.8%. At the same time, the calculated value of efficiency for monochromatic light is 6.8%. With allowance for the good coincidence between the calculated and measured efficiencies at maximal powers, we can state that this difference at low powers is caused by the amplitude modulation of laser light.

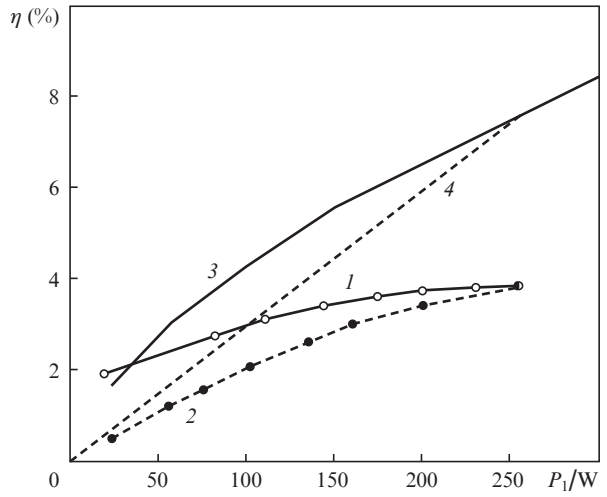

Figure 7. (*1*, *2*) Measured and (*3*, *4*) calculated dependences of conversion efficiency for a focused FH beam with $a_{min} = 14$ μm in a 9-mm-long KTP crystal on the (*1*, *3*) lasing power and (*2*, *4*) the FH power, varied using a polarisation attenuator at a constant lasing power of 250 W and an FH spectral width of 30 cm^{-1}.

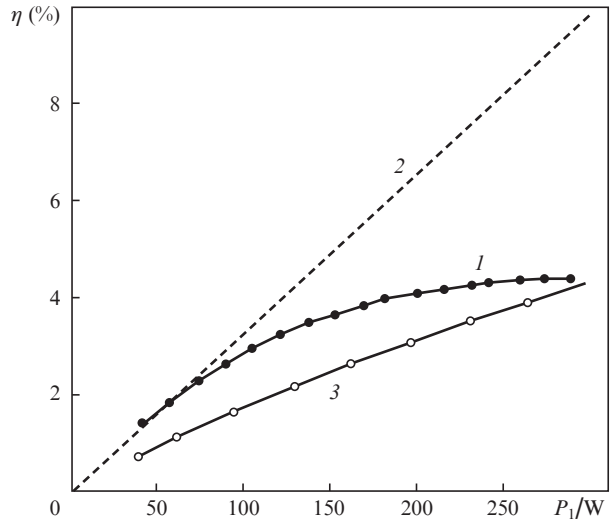

Figure 8. (*1*) Experimental dependence of the SH conversion efficiency in an LBO crystal on the lasing power in the cw regime; (*2*) extrapolation of the efficiency measured at $P_1 = 30$ W and an FH spectral width of 5.6 cm^{-1} to the efficiency at 300 W, provided that the FH linewidth is 5.6 cm^{-1}; and (*3*) the conversion efficiency obtained by calculation taking into account the experimental lasing spectrum.

Figure 10 shows the dependence of the normalised conversion efficiency on the LBO crystal temperature at a maximum spectral width and an FH power 300 W, as well as at a minimum spectral width and an FH power of 30–40 W. The data obtained make it possible to determine the phase matching curve width Δf_{s1} and, therefore, verify the value of the group-velocity mismatch S_{21} that was reported in [10]. To this end, the obtained temperature dependences of the conversion efficiency can evidently be recalculated into the corresponding spectral dependences using the temperature spectral coefficient $\alpha_{Tf} = 0.139\,^{\circ}\mathrm{C\ cm^{-1}}$. Since all these dependences, as follows from (1), are convolutions of the nonlinear polarisation spectrum $p_{2\omega}(f_1)$ and the phase matching curve $S(\Delta k(f_1))$ and all curves are close to Gaussian in the central part, the spectral width of the measured curve of conversion efficiency Δf_T can be expressed in terms of the corresponding spectral widths as follows: $\Delta f_T = [(\Delta f_{p2}/2)^2 + (\Delta f_{s1})^2]^{1/2}$. At the maximum power of FH and its spectral width $\Delta f_1 \equiv 33.6\ \mathrm{cm^{-1}}$, the width of experimental curve *1* in Fig. 10 is $\Delta T = 6.4\,^{\circ}\mathrm{C}$ or (recalculated to frequency) $\Delta f_T = 46\ \mathrm{cm^{-1}}$. Taking into account that in the case of high FH power $\Delta f_{p2}/\Delta f_1 \approx 2$, we obtain $\Delta f_{s1} = 31.4\ \mathrm{cm^{-1}}$. This value is in good agreement with the value $\Delta f_{s1} = 31.4\ \mathrm{cm^{-1}}$, calculated based on the data of [10], and with the previously calculated value of $30.9\ \mathrm{cm^{-1}}$. At low lasing power and, correspondingly, small spectral width, $\Delta f_1 \equiv 5.6\ \mathrm{cm^{-1}}$ and the temperature width ΔT [see curve (*2*) in Fig. 10] is $4\,^{\circ}\mathrm{C}$ (or $\Delta f_T = 28.9\ \mathrm{cm^{-1}}$). Hence, assuming that $\Delta f_{p2}/\Delta f_1 = 3$, we obtain $\Delta f_{s1} = 27.7\ \mathrm{cm^{-1}}$. The deviation of this value from that determined above is apparently due to the smaller beam radius at the output laser collimator in this operation regime.

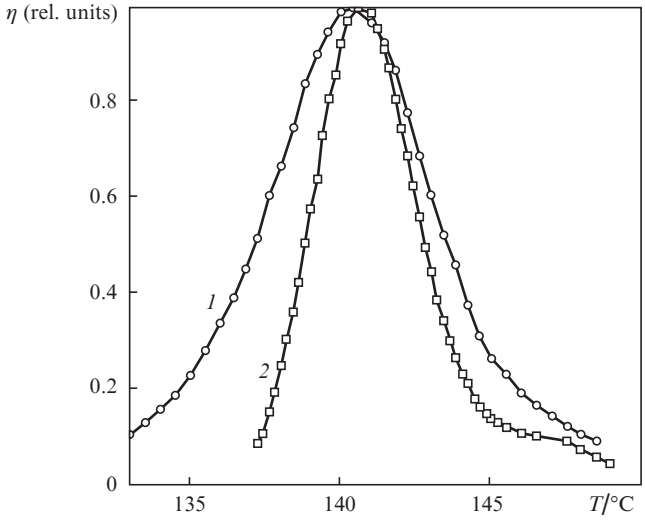

Figure 9. Experimentally normalised temperature dependences of the SHG efficiency in an LBO crystal for (*1*) broadband FH radiation with $\Delta f_1 = 33.6\ \mathrm{cm^{-1}}$ and $P_1 = 300$ W and (*2*) narrow-band radiation with $\Delta f_1 = 5.6\ \mathrm{cm^{-1}}$ and $P_1 = 30–40$ W.

4.2. Two-stage doubler

In the experimental implementation of the above-proposed scheme with compensation of the phase mismatch of broadband harmonic fields, we met the problem of accurate calculation of the α-BBO crystal thickness at which all group delays of harmonics in the scheme elements will be compensated and the alignment will be reduced to only rotation of the α-BBO crystal to compensate for the phase shifts of carrier frequencies. This is related to the error in calculating the group velocities in the optical elements using the known spectral dependences of the refractive index for LBO and α-BBO crystals and crystalline quartz and fused silica. In this context, we supplemented the optical scheme with two oppositely oriented fused silica wedges, which were mounted near the α-BBO plate (Fig. 1); the total thickness of these wedges at their relative transverse shift could be varied from 5 to 8 mm. The distance between the image transfer system lenses was aligned for each total optical thickness of the wedges at the SH frequency. In addition, we prepared an α-BBO plate with a thickness of 5.5 mm, which obviously exceeded the value necessary for the initial scheme.

During the alignment, we recorded the dependence of the SHG efficiency on the angle of rotation of the α-BBO plate [which changed the $\Psi(0)$ value] at each chosen total thickness of wedges. As a result, we chose a thickness at which the aforementioned dependence, in correspondence with formula (5), exhibited the largest contrast between the maximum and minimum SH conversion efficiencies, attained at certain $\Psi(0)$ values. Figures 11a and 11b present the transverse distributions of the SH intensity at the output of the second NLC in the interference maximum and minimum, respectively; they were recorded using the BeamStar FX 50 system (Ophir). The distribution in Fig. 11a is in fact an ideal Gaussian curve. The distribution in Fig. 11b, which was recorded in the interference minimum at strong suppression of SH fields, at the limit of video camera sensitivity, reveals aberrations of SH beams, which cannot be compensated for by coherent subtraction of fields. It can be seen that complete beam suppression is observed along the cross-shaped region, located in the diagonal in the photograph. Figure 11c shows as an example of the transverse structure of the SH beam, which was obtained using a chromatic-aberration image transfer system, composed of VK-7 glass lenses. One can see a ring structure, which is due to the difference in the radii of curvature of the SH fields excited in different crystals. In this case, the increase in the efficiency after the second cascade was about 2.1; it depended weakly on the angle of rotation of the α-BBO crystal plate.

The use of silica wedges with a variable total thickness and α-BBO plates of different thicknesses in the two-stage scheme allowed us to determine the normalised group mismatches in the α-BBO and LBO crystals in measurements similar to the above-described ones. On the assumption that $S_{21} = 0.022603$ for fused silica and $S_{21} = 0.016856$ for crystalline quartz (these values were obtained from the well-known Sellmeier formulas), our measurements for the LBO crystal at a noncritical phase-matching temperature yielded $S_{21} = 0.0120$, a value coinciding with that found using the SNLO code [10]. For the α-BBO crystal, $S_{21} = -0.0918$, which differs from the values of -0.1074 and -0.08574, calculated from the formulas [16, 17], by 17% and 6.7%, respectively. The error of our measurements did not exceed 2.5%.

We also measured the dependence of the SH conversion efficiency on the lasing power in the two-stage scheme [Fig. 12, curve (*2*)]. The power was varied by controlling the pump diode current. Curves (*2*) and (*3*) indicate that the two-stage converter efficiency exceeds that in the first NLC by a factor of 3.3 in the entire range of powers and the corresponding linewidths; a fact suggesting weak influence of the image transfer system chromatic aberrations. The increase obtained by us (by a factor of 3.3) is below the ultimate (four-

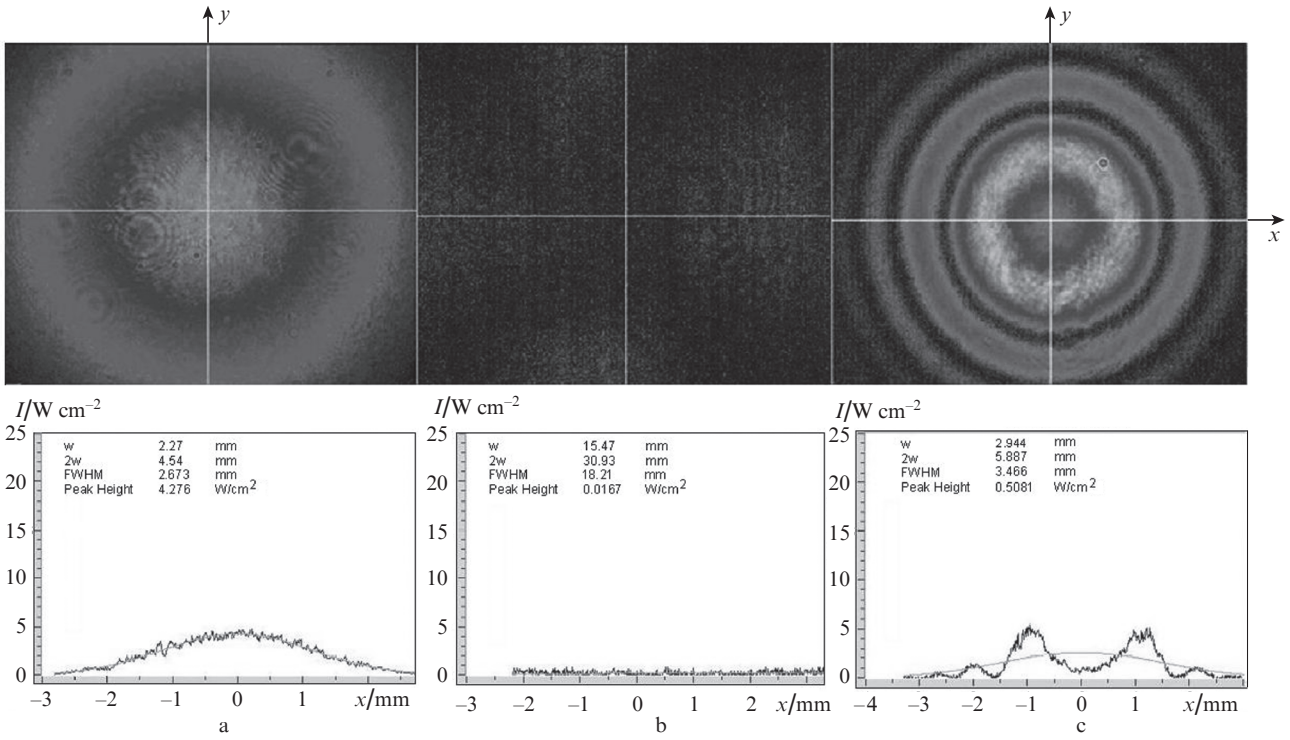

Figure 10. Photographs and profiles of the transverse cross section of a SH beam at the output of the second crystal for image transfer systems with (a, b) achromatic and (c) chromatic lenses: (a) SH beam in the interference maximum, (b) SH beam in the interference minimum, and (c) the ring structure of SH beam when an image transfer system with chromatic lenses is used (the bright curve is a Gaussian approximation of the experimental dependence).

fold) increase mainly because of the FH and SH radiation loss in the image transfer system elements (the FH and SH transmittances are, respectively, $T_1 = 0.96$ and $T_2 = 0.88$). At a total laser power of 290 W at the input of the scheme, the conversion coefficients of the crystals used were as follows: $\eta_1 = 3.4\%$ in the first NLC and $\eta_2 = 3.2\%$ in the second NLC. At a maximum pulse power $P_1 = 290$ W and the FH spectral width $\Delta f_1 = 33.6$ cm^{-1}, the ratio of the SH power in the maximum of dependence (5) to the SH power in its minimum (the contrast coefficient) was ~50. Calculation (by the same formula) of the overlap coefficient in the interference minimum, i.e., at $\cos(\Psi(0)) = -1$, yielded $H_{1,2} \geqslant 0.966$ for the two-stage scheme. It is noteworthy that, assuming $\cos(\Psi(0)) = +1$ and $H_{1,2} = 0.966$ in (5), we find the total efficiency η_Σ in the interference maximum to be 11.9%. This value exceeds the measured maximum efficiency by 4%. Note also that Gehr et al. [5], who doubled frequency of 250-fs pulses in two β-BBO crystals (using β-BBO plates to compensate for the group walk-off), increased the efficiency (in comparison with the single-crystal case) by a factor of 2.85. The FH radiation was focused into the system of crystals without a image transfer system, as in [6].

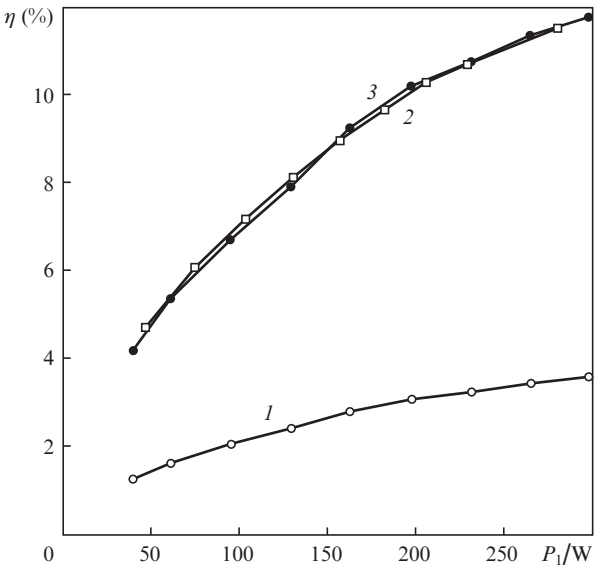

Figure 11. Experimentally measured SH conversion efficiencies as functions of the peak power of a 100-μs FH pulse in the repetitively pulsed regime of a fibre laser in one LBO crystal (*1*) and two crystals placed in series (*2*), as well as the efficiencies corresponding to curve (*1*), magnified by 3.3 times (*3*).

4.3. Three-stage doubler

We studied the three-stage doubling scheme, which is formed from a two-stage one by locating a third cascade (composed of a similar image transfer system and an LBO crystal in thermostat) after the second cascade. The SH conversion efficiency in the third NLC, η_3, at an FH power of 272 W at its input, was 2.8%. It is somewhat smaller than the calculated value of 3%, which is determined by the loss of FH power during propagation through the image transfer system elements; however, it is within the experimental error. When doubling in the second and third crystals in the absence of SHG in the first crystal, the field overlap factor $H_{2,3} \geqslant 0.956$,

and the ratio of the maximum and minimum efficiencies is 36.5 (i.e., somewhat smaller than in the first and second crystals). This could be caused by the aberrations introduced by the additional optical elements. The measured efficiency in the interference maximum (10.2%) was lower than the value calculated at $H_{2,3} = 0.956$ in correspondence with (5) by 5%.

The total conversion efficiency of the three cascades in the interference maximum was $\eta_{1,2,3} = 17.1\%$, a value corresponding to the increase in the SH conversion efficiency in the three-stage scheme with real loss by a factor of 4.9 in comparison with the efficiency of the first NLC.

Measurement of the SH powers at the output of the first two cascades and then (separately) in the third crystal, with the first and second crystals out of the phase-matching conditions (i.e., in the absence of SHG in them), as well as at the output of all cascades in the interference minimum, gave [in correspondence with (5)] the field overlap factor $H_{1,2,3} \geqslant 0.924$. At this value, the efficiency in the interference maximum, in correspondence with the same formula, should be 21.7%. The deviation of the measured value from the calculated one exceeds the measurement error by a factor of 1.27. This fact indicates significant influence of the saturation effect in the third cascade on the SHG efficiency in the three-stage converter.

Using the measured overlap coefficients, one can predict the increase in the SH conversion efficiency in two- and three-stage schemes in the absence of power loss in the optical elements of image transfer systems, with allowance for real beam aberrations but disregarding the conversion saturation. For the two-stage scheme this increase is calculated, in correspondence with (5), from the formula $B_{1,2} = 2 + 2H_{1,2} = 3.9$; for the three-stage scheme, the calculation is performed based on the formula $B_{1,2,3} = \left[2 + 2H_{1,2} + 1 + 2H_{1,2,3}\sqrt{2 + 2H_{1,2}}\right] = 8.6$. This means that, for cw broadband polarised radiation with an average power $P_1 \approx 300$ W and spectral width $\Delta f_1 = 33$ cm^{-1}, a two-stage converter yields a conversion efficiency $\eta_{1,2} = 17.5\%$ and a SH power of 52 W; for the three-stage scheme, $\eta_{1,2,3} = 38.7\%$ and $P_2 \approx 116$ W. With allowance for saturation in the third cascade, the predicted values for the three-stage converter may decrease by a factor of about 1.3, i.e., to $B_{1,2,3} = 6.6$, $\eta_{1,2,3} \approx 30\%$, and $P_2 \approx 90$ W.

5. Conclusions

A new scheme of a cascaded converter of broadband cw first-harmonic radiation into the second harmonic, with compensation for the group walk-off in the cascades, was proposed and investigated.

The relations obtained in the fixed-field approximation for broadband phase-modulated FH radiation made it possible to analyse the dependence of the SHG efficiency (when focusing this radiation in an NLC) on its spectral width and the degree of focusing, as well as on the NLC parameters.

The same approximation was used to analyse the operation of two- and three-stage converters with image transfer systems and anisotropic plates between cascades to match the group walk-off of FH and SH radiation. The analysis was performed taking into account the loss in the image transfer systems, incomplete spatial and temporal overlap of the SH radiation excited in the cascades, and its phase mismatch. Relations between the total conversion efficiency of the converter and the conversion efficiencies of individual cascades were obtained.

The analysis performed showed that the LBO crystal is most promising for doubling the frequency of radiation with an average power of ~300 W and a spectral width of ~33 cm^{-1}.

When doubling the frequency of broadband ($\Delta f_{1\omega} \approx 33$ cm^{-1}) nonpolarised laser radiation with an average power of ~600 W, we obtained polarised SH radiation of power $P_2 = 13.5$ W with a polarised-component conversion efficiency $\eta_2 = 4.5\%$ in a converter based on a single LBO crystal. This efficiency is close to the value calculated on the assumption that the FH is phase-modulated. In this case, the radiation load reached 100 MWcm^{-2} in the region of FH-beam waist and 10 MWcm^{-2} on the NLC end faces. The latter value is close to the breakdown threshold for the LBO crystal surface.

An experimental study of the two-stage frequency doubler based on an LBO crystal with an α-BBO compensating plate and quartz wedges for alignment showed the following: to calculate correctly the compensating-plate thickness, one must use the group walk-off value $S_{21} = -0.0918$ for α-BBO, which we believe to be more exact than that reported in [3, 4].

When doubling frequency of pulse-modulated radiation (~100-μs rectangular pulses, spectral width $\Delta f_1 \approx 33$ cm^{-1}) of power $P_1 = 300$ W in a two-stage doubler, we obtained an increase in the conversion efficiency by a factor of 3.3, which is smaller than the ultimate (fourfold) increase (mainly because of the loss in the image transfer system). Elimination of this loss will make it possible to increase the gain due to application of a two-cascade converter to 3.9, i.e., obtain $\eta_{1,2} \approx 17.5\%$ and $P_2 \approx 53$ W at frequency doubling of cw broadband radiation with an average power $P_1 = 300$ W.

Similar measurements for a three-stage converter gave an increase in the conversion efficiency in comparison with the single-stage converter by a factor of 4.9. An analysis of the experimental data showed that this value can be controlled by the significant effect of FH depletion in the third cascade. If this effect is disregarded and the loss in the image transfer systems is eliminated, one would expect three-stage SHG to increase the conversion efficiency by a factor of 8.9 and, correspondingly, yield the values $\eta_{1,2,3} \approx 38.7\%$ and $P_2 \approx 116$ W for cw broadband polarised radiation with an average power $P_1 \approx 300$ W and spectral width $\Delta f_1 \approx 33$ cm^{-1}. With allowance for the pump depletion in the third cascade, the predicted values for the three-stage converter may decrease by a factor of about 1.3, i.e., to $B_{1,2,3} = 6.6$, $\eta_{1,2,3} \approx 30\%$ and $P_2 \approx 90$ W.

Acknowledgements. We are grateful to V.V. Lozhkarev for his help in spectral measurements.

References

1. Hong K.H., Lai C.J., Siddiqui A., Kärtner F.X. *Opt. Express*, **17**, 6911 (2009).
2. McDonagh L., Wallenstein R., Nebel A. *Opt. Lett*., **32**, 1259 (2007).
3. Liu A., Norsen M.A., Mead R.D. *Opt. Lett*., **30**, 67 (2005).
4. Kojima T., Fujikawa S., Yasui K. *IEEE J. Quantum Electron*., **35**, 377 (1999).
5. Gehr J.G., Kimmel M.K., Smith A.V. *Opt. Lett*., **23**, 1298 (1998).
6. Smith A.V., Armstrong D.J., Alford W.J. *J. Opt. Soc. Am. B*, **15,** 122 (1998).
7. Freidman G.I. *Izv. Vyssh. Uchebn. Zaved., Ser. Radiofiz*., **54**, 41 (2011).
8. Boyd G.D., Kleinman D.A. *J. Appl. Phys*, **39**, 3597 (1968).

9. Dmitriev V.G., Tarasov L.V. *Prikladnaya nelineinaya optika* (Applied Nonlinear Optics) (Moscow: Fizmatlit, 2004).
10. SNLO Nonlinear Optics Code available from A.V.Smith. Sandia National Laboratories, Albuquerque. NM 87185-1423.
11. Velsko S., Webb M., Davis L., Huang C. *IEEE J. Quantum Electron*., **27**, 2182 (1991)
12. Kiriyama H., Nakano F., Yamakawa K. *J. Opt. Soc. Am. B*, **19**, 1857 (2002).
13. Kokh A., Kononova N., Mennerat G., et al. *J. Crystal Growth*, **312**, 1774 (2010).
14. Zel'dovich B.Ya., Kapitskii Yu.E., Chudinov A.N. *Kvantovaya Elektron.*, **17**, 1212 (1990) [*Sov. J. Quantum Electron*., **20**, 1120 (1990)].
15. Andreev N.F., Vlasova K.V., Davydov V.S., et al. *Sb. dokl. 3-i Vseros. shkoly dlya studentov, aspirantov, molodykh spetsialistov po lazernoi fizike i lazernym tekhnologiyam* (Proc. 3rd All-Russia School for Students, Postgraduates, and Young Experts in Laser Physics and Laser Technologies) (Sarov, 2009) p. 93
16. http://www.agoptics.com/Birefrigent-Crystal/alpha-BBO.htm.
17. http://www.crystech.com/products/crystals/birefringentcrystals/a-BBO.htm.